

Article

Nanoencapsulated Myricetin to Improve Antioxidant Activity and Bioavailability: A Study on Zebrafish Embryos

Gopikrishna Agraharam, Agnishwar Girigoswami  and Koyeli Girigoswami * 

Faculty of Allied Health Sciences, Chettinad Hospital and Research Institute, Chettinad Academy of Research and Education, Kelambakkam 603103, Tamilnadu, India; agopikrishna4912@gmail.com (G.A.); agnishwarg@gmail.com (A.G.)

* Correspondence: koyelig@gmail.com or koyelig@care.edu.in; Tel.: +91-960-0060-358; Fax: +91-0-444-7411-011

Abstract: Flavonoids are natural polyphenolic compounds that mainly possess antioxidant properties due to more hydroxyl groups in their structure and play an important role in combatting many diseases. Myricetin is a flavonoid found in grapes, green tea, fruits, and vegetables and is not only an antioxidant but also is a pro-oxidant. Myricetin is sparingly soluble in water and restricts its properties due to low bioavailability. The present study reports the liposomal nanoformulations of myricetin to improve its bioavailability with reduced pro-oxidant activity. The nanoformulated myricetin was characterized using different photophysical tools, such as dynamic light scattering (DLS), zeta potential, and scanning electron microscopy (SEM). The effect of nanoencapsulated myricetin on the developing zebrafish embryo was studied in terms of microscopic observations, cumulative hatchability, and antioxidant activities, such as catalase, glutathione peroxidase, and superoxide dismutase, after treating the zebrafish embryo with standard oxidant hydrogen peroxide. The results obtained from the cumulative hatchability, developmental studies, and antioxidant assays indicated that the liposomal nanoformulation of myricetin had enhanced antioxidant activity, leading to defense against oxidative stress. The formulation was highly biocompatible, as evidenced by the cumulative hatching studies as well as microscopic observations. The positive effects of liposomal nanoformulation on zebrafish embryos can open an avenue for other researchers to carry out further related research and to check its activities in clinical studies and developmental studies.

Keywords: myricetin; liposomal nanoformulation; zebrafish embryos; antioxidant enzyme activity; cumulative hatchability; oxidative stress



Citation: Agraharam, G.; Girigoswami, A.; Girigoswami, K. Nanoencapsulated Myricetin to Improve Antioxidant Activity and Bioavailability: A Study on Zebrafish Embryos. *Chemistry* **2022**, *4*, 1–17. <https://doi.org/10.3390/chemistry4010001>

Academic Editors: Simona Fabroni, Krystian Marszałek and Aldo Todaro

Received: 19 November 2021

Accepted: 29 December 2021

Published: 31 December 2021

Publisher's Note: MDPI stays neutral with regard to jurisdictional claims in published maps and institutional affiliations.



Copyright: © 2021 by the authors. Licensee MDPI, Basel, Switzerland. This article is an open access article distributed under the terms and conditions of the Creative Commons Attribution (CC BY) license (<https://creativecommons.org/licenses/by/4.0/>).

1. Introduction

Free radicals are ubiquitous in our environment, and our body is exposed to them daily. Oxygen-centered radicals cause oxidative stress and are produced due to endogenous sources as a result of metabolism as well as exogenous sources, such as exposure to smoke and radiation. Thus, we are continuously exposed to oxidative stress (OS). To combat this OS, organisms have a defense system mediated by antioxidant enzymes and molecules. However, some of the free radicals escape from these antioxidant defense systems, due to which we are exposed to a chronic low dose of oxidants, which is the etiology of cancer [1,2]. Nutraceuticals are available from different foods, fruits, and vegetables and have been shown to possess an antioxidant capacity. Thus, supplementation with these nutraceuticals can enhance the capacity to fight against oxidative stress [3,4]. Myricetin falls under the group of flavonols and is found in food items such as vegetables, fruits, and tea and has shown potent activity against many radicals, even at low concentrations, compared to other flavonoids [5,6]. The myricetin structure has two aromatic rings, A and B, that are combined by a three-carbon chain forming a cyclic ring C, and reports suggest that the presence of more hydroxyl groups is one of the reasons for myricetin to be a potent antioxidant [7]. The drawback of myricetin being used for oral consumption is that it is poorly soluble in

water and its bioavailability is low. Other than protective effects, myricetin also shows pro-oxidant activity, which is harmful to the cells as well as biomolecules [8].

Nanotechnology is a field of science that is emerging rapidly, yielding enormous applications in the biomedical field for the treatment of many diseases, such as Alzheimer's disease and Parkinson's disease [9,10]. The different physical parameters, such as pH and temperature, can be altered to tune the size and surface properties of these nanostructures [11,12]. Different nanostructures include liposomes, micelles, nanoparticles, nanosheets, nanorods, solid lipid nanoparticles, niosomes, vesicles, microporous silica, magnetic nanoparticles, metal, and metal-oxide-based nanoparticles [13–17]. Even though there are reports on increased myricetin bioavailability that is encapsulated in microemulsions, prepared from oil, water, surfactant and co-surfactant [18], and solid lipid nanoparticles (SLNs) [19], there exist many drawbacks, which warrants the development of new approaches for myricetin encapsulation. Microemulsions are responsive to temperature and salinity changes and may undergo phase changes when exposed to higher- or lower-than-normal temperatures or salinity concentrations. This could lead to breaking of the microemulsion and, eventually, phase separation. Because of their crystalline structure and crystallization process, SLNs have drawbacks, such as low drug loading efficiency, possibilities of drug expulsion in storage conditions, and initial burst release.

In this study, to offer improved nanoformulation, we encapsulated myricetin in liposomes and observed its antioxidant activity in zebrafish embryos after treatment with hydrogen peroxide (H_2O_2). H_2O_2 was used to induce oxidative stress in the embryos, which were pre-treated with only myricetin and nano-myricetin. Antioxidant enzyme activities, such as catalase (CAT), superoxide dismutase (SOD), and glutathione peroxidase (GPx), were assayed. To study the effect of myricetin on the developmental stages, we also observed the embryos microscopically and calculated the cumulative hatchability posttreatment with H_2O_2 and H_2O_2 pre-treated with only myricetin and nanoencapsulated myricetin. The work was executed to yield a superior product using liposomal nanoencapsulation that can be more biocompatible and bioavailable to exert its antioxidant effect.

2. Materials and Methods

2.1. Materials Used

Myricetin was purchased from TCI, Japan (Purity > 97.0%); ethanol, methanol, and chloroform were from E Merck; cholesterol, trypsin, collagenase, and DPPH were procured from HiMedia Laboratories Pvt Ltd.; and PBS tablets, sodium chloride (NaCl), ascorbic acid, dialysis membrane, and other chemicals were procured locally.

2.2. Isolation of Phospholipids from Egg Yolk

The yolk was collected from a hen egg, and phospholipids were isolated according to Ramesh et al. [20] with slight modification. To 1 mL of egg yolk, 3 mL of 1 M NaCl was added and the mixture vortexed for proper mixing, followed by the addition of 12 mL of a methanol:chloroform mixture (2:1 ratio). The contents were mixed vigorously using a vortex. Further, 1 mL of 1 M NaCl and 3 mL of chloroform were added and the mixture vortexed. Later, this mixture was centrifuged at 2000 rpm for 5 min, which separated the mixture into three phases. The bottom organic phase was collected, which had pale-yellow-colored phospholipids, and was stored at $-20\text{ }^\circ\text{C}$ for thin-layer chromatography (TLC) confirmation.

2.3. Confirmation of Phospholipids by Thin-Layer Chromatography

TLC plates were activated after heating at $110\text{ }^\circ\text{C}$ for 30 min. A line was drawn at the bottom, 0.5 cm above the edge, without scratching the gel and marked as the origin. With the help of a capillary tube, the extracted phospholipid was loaded at the center of the marked line and allowed to dry. Loading was repeated four times. The developing solvent was made by adding chloroform, methanol, and water in a ratio of 400:90:5 (i.e., chloroform:methanol:water = 8 mL:1.8 mL:0.1 mL) and placed in a beaker covered with a

tight lid. After the loading of the sample was over, it was placed in the beaker and allowed to develop. When the solvent front reached near the top, the TLC plate was removed and the solvent front was marked. After drying in air, the TLC plates were placed in a large beaker containing iodine crystals and covered. After 15 min, the spots were stained in brown. The solvent front and sample spots were marked.

2.4. Nanoencapsulation of Myricetin

We used the procedure of Gaber et al. [19] and Vimaladevi et al. [21] for the nanoencapsulation of myricetin with slight modification. We added 5 μL of phospholipids, which were isolated from egg yolk, and 2 mg of cholesterol to an RB flask. To this, the methanol and chloroform mixture was added in a 1:3 ratio (2 mL of methanol:6 mL of chloroform). Then, 5 mg of myricetin, which was dissolved in 2 mL of methanol, was added to the RB flask. This complete mixture was evaporated by using a rotatory evaporator, and liposome-encapsulated myricetin was formed as a thin film inside the flask walls. Later, the RB flask with the thin film was kept under overnight incubation at room temperature in a desiccator for complete drying of the solvent. To prepare the liposome, the same process was executed without the addition of myricetin. The next day, we added 25 mL of PBS to the formed thin film in the RB flask and sonicated it for 20 min at room temperature. Then we filtered the sample with a 0.45 μm filter and stored it at 4 $^{\circ}\text{C}$ for further use. The characterization for size and stability was performed by dynamic light scattering using a Malvern zeta sizer. To explore the surface morphology of the liposome-encapsulated myricetin (n-Myr), we performed scanning electron microscopy (SEM). A thin layer of n-Myr was made above a solid support and dried in a dust-free atmosphere. Surface scanning was performed using JEOL JEM 2100 HRTEM with an accelerating voltage of 200 kV.

2.5. Drug Release Kinetics

The drug release kinetics of n-Myr was analyzed according to Deepika et al. [22] using a dialysis membrane in a phosphate buffer saline (1X, pH 7.4) at room temperature. n-Myr (250 μM) was loaded in a dialysis membrane, and the membrane was placed in a beaker containing 50 mL of PBS solution (pH = 7.4). At specific time intervals, 2 mL of the released-n-Myr-containing buffer solution was withdrawn and the same volume of fresh PBS was added to maintain the total volume. The amount of released myricetin (Myr) was measured spectrophotometrically by measuring the absorbance at 324 nm. The encapsulation efficiency (EE) of n-Myr was evaluated spectrophotometrically [22].

2.6. Free-Radical-Scavenging Activity

The free-radical-scavenging activity of Myr and n-Myr was determined by using DPPH assay with two different concentrations of Myr (50 μM and 250 μM) and n-Myr (50 μM and 250 μM). The free-radical-scavenging activity of the zebrafish embryo cell lysate was also assessed. Briefly, zebrafish embryos (10 embryos) were taken for each treatment group and treated with only liposomes without myricetin and individually with Myr-L, Myr-H, n-Myr-L, and n-Myr-H for 24 h. Untreated embryos were taken as controls. Treatment with H_2O_2 (3 mM) was performed after 24 h, and DPPH radical scavenging was carried out immediately after treatment and 2 h after treatment. Posttreatment, the embryos were converted into a single-cell suspension using a combination of trypsin and collagenase, as described by Bresciani et al. [23]. Then the cells were lysed with lysis buffer (50 μM potassium phosphate buffer containing 0.5% Triton X-100) and the cell lysate (50 μL) was added to 2 mL of 100 μM DPPH. Absorbance was measured at 517 nm after 0 min and 30 min. Here, 50 mM ascorbic acid was taken as a positive control. The percentage of the free-radical-scavenging activity of cell lysate was measured according to the percentage of the inhibition formula [24].

$$\% \text{ of inhibition} = A_0 - A_{30}/A_0 \times 100$$

A_0 = OD at 0th minute.

A30 = OD at 30th minute.

2.7. *Culturing, Breeding of Zebrafish, and Collection of Embryos*

Male and female zebrafish (*Danio rerio*) were cultured in a rectangular fish tank according to Girigoswami et al. [25] with slight modifications, by supplementing blood worms and flakes as food 2 times per day at room temperature (27 °C) in 12 h/12 h light/dark conditions. Care was taken, and the tank was cleaned once a week. To collect embryos, female and male zebrafish (3:4 ratio) were transferred into one fish tank in the evening and left for spawning. The next day, the embryos that were at the bottom of the tank were collected, washed with distilled water thrice, and used for the study.

2.8. *Myricetin and Nanoformulated Myricetin Treatment*

After collecting and washing the zebrafish embryos, we took 10–20 embryos in each well of the two 6-well plates. These wells we divided into 5 groups (control, myricetin low dose, myricetin high dose, nano-myricetin low dose, and nano-myricetin high dose) in duplicates (total 10 wells, 5 in one plate for treatment). The total volume of the solution in each well was 3 mL. We added 3 mL of distilled water (DIW) to the control group; then the final concentration of myricetin and nano-myricetin in low dose and high dose was 50 µM and 250 µM, adjusted with water and stock solutions of myricetin and nano-myricetin, respectively. The embryos were incubated for 20 h at room temperature (25 °C). Then the embryos were washed with distilled water twice, and all wells were filled with 3 mL of distilled water.

2.9. *Hydrogen Peroxide Treatment*

To observe the protective effect of myricetin and nano-myricetin against oxidative stress (OS), H₂O₂ was taken as a source of oxidant. After washing the embryos, we added 3 mM H₂O₂ to the myricetin- and nano-myricetin-treated embryos in each well to induce oxidative stress in the 6-well plate and incubated for 2 h at room temperature. After 2 h H₂O₂ treatment, the embryos were washed with distilled water twice and then filled with 3 mL of distilled water and incubated at room temperature. The embryos not treated with H₂O₂ were taken as a control.

2.10. *Developmental Observations Using Microscopy*

After H₂O₂ treatment, every day, embryos were analyzed under an inverted microscope. Due to the transparency of zebrafish embryos, we assessed the effect of myricetin and H₂O₂ on zebrafish embryos.

2.11. *Cumulative Hatching*

The cumulative hatchability was calculated, as performed previously [25]. After the treatment, the embryos were incubated at room temperature and the number of hatched zebrafish embryos was noted in each well for 4 days. The embryos in each well at each time were calculated using the formula

$$\% \text{ of cumulative hatching} = (\text{Hatched embryos} / \text{Total embryos}) \times 100.$$

A graph was created by taking time in hours postfertilization (hpf) on the abscissa and the percentage (%) of cumulative hatching on the ordinate according to Girigoswami et al. [25].

2.12. *Assay of Antioxidant Activities*

Protein was estimated according to Lowry's method. The antioxidant defense was assayed in H₂O₂-untreated and H₂O₂-treated zebrafish embryos that were pre-treated for 20 h with myricetin low dose (50 µM) and high dose (250 µM) and liposome-encapsulated myricetin low dose (50 µM) and high dose (250 µM). Antioxidant enzymes, such as CAT, GPx, and SOD, were assayed according to Girigoswami et al. [2]. Both 2 h H₂O₂-treated and

H₂O₂-untreated embryos were washed twice with distilled water and taken as respective controls. Calculations were carried out for antioxidant assays based on Girigoswami et al. [2].

2.13. Catalase and Glutathione Peroxidase Assay

For catalase (CAT) and glutathione peroxidase assays from every group, we collected 10 embryos into the glass homogenizer and suspended them in lysis buffer (~300 µL) (50 µM potassium phosphate buffer containing 0.5% Triton X-100) and the homogenizer was kept on ice for 15 min for lysis of embryos. Then we homogenized the embryos with a piston by keeping the homogenizer on ice to maintain the temperature at 4 °C to hold enzyme activities until assay. We collected 50 µL of the lysate for protein estimation from each group of embryos. The protein estimation was performed with less volume of cell lysate (50 µL) by Lowry's method (1951).

Then, the remaining extracted sample was centrifuged for 5 min at 800 × *g* at 4 °C, and the supernatant was taken for catalase assay by following the procedure of Claiborne [26] and for glutathione peroxidase assay by following the method of Gunzler and Flohe [27].

2.14. Superoxide Dismutase Assay

To assay the amount of SOD present in different cellular extracts, the SOD standard curve was drawn by plotting the amount of pure SOD (ng) vs. the percentage of NADH oxidation. The procedure followed was essentially the same as that by Paoletti et al. [28]. A stock solution of standard SOD 100 µg/mL was prepared, and the amount was varied from 10 ng to 90 ng for the experiment. To find the SOD level, 10 zebrafish embryos were taken from each group and added to the homogenizer each time, and we added 600 µL of 100 mM TEA-DEA buffer (triethanolamine 665 µL from the stock of 1.12 kg/L, diethanolamine 480 µL from the stock of 1.091 kg/L, and HCl 690 µL (37%) were mixed and made up to 50 mL with d.H₂O; pH maintained at 7.4–7.5) and kept on ice for 15 min. Then the embryos were homogenized by keeping them on ice to avoid loss of enzyme activity. To remove low-molecular-weight substances, the supernatant was loaded into a Sephadex G-25 (coarse) column and sieved by centrifugation at 18,000 rpm for 5 min at 4 °C. The eluant contained the sample, which was immediately transferred to ice. From each sample, 3 µL of the supernatant was collected for protein estimation by Lowry's method and the remaining supernatant was used for SOD assay by keeping it on ice until completion of SOD assay. Volumes from this supernatant were used for SOD measurement according to Paoletti et al. [28].

2.15. Statistical Analysis

All the experiments were performed in triplicate. Student's *t*-test was used to find the significance between the values.

3. Results

3.1. Isolation of Phospholipid from Egg Yolk

Figure 1 shows that there were two bands in the thin-layer chromatogram. The two bands represented the two components of phospholipids present in egg yolk phosphatidylethanolamine and phosphatidylcholine, which are represented by arrows in the figure.

3.2. Characterization of the Nanoencapsulated Myricetin

The inverted microscopic images of myricetin and liposome-encapsulated myricetin are given in Figures S1 and S2, respectively. The characterization for size and stability was performed by dynamic light scattering using a Malvern zeta sizer. The liposomes had a hydrodynamic diameter of 212 nm and a zeta potential of −30.2 mV, which shows that they were highly stable. The hydrodynamic diameter of the nanoencapsulated myricetin was 262 nm, and its zeta potential was −20.2 mV (Table 1), and this formulation was used for further study. The zeta potential of −20.2 mV showed that nanoencapsulated myricetin is highly stable. The hydrodynamic diameter of 262 nm also indicated that the

nanoformulation was in the range of nanometers. The encapsulation efficiency of myricetin in liposomes was found to be 72%.

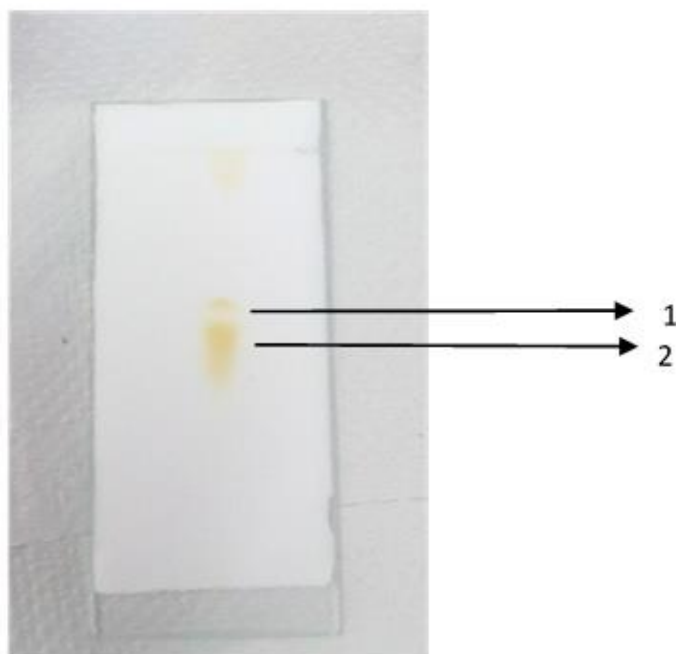


Figure 1. The thin-layer chromatogram of the phospholipids isolated from egg yolk. The two bands indicate phosphatidylethanolamine (band 1) and phosphatidylcholine (band 2), which are the components of phospholipids.

Table 1. The hydrodynamic diameter and zeta potential of liposomes and liposomal-nanoencapsulated myricetin.

Sample	Hydrodynamic Diameter (nm)	Zeta Potential (mV)
Liposomes	212	−30.6
Liposomal-nanoencapsulated myricetin	262	−20.2

3.3. Drug Release Kinetics

The drug release kinetics of n-Myr is shown in Figure 2. The release was shown nearly 80% after 3 h.

3.4. Scanning Electron Microscopy and Free-Radical-Scavenging Activity

The surface morphology of n-Myr is shown in Figure 3A. The shape was perfectly spherical, and the size of the synthesized n-Myr ranged from 90 to 120 nm. The free-radical-scavenging activity is shown in Figure 3B for low and high doses of Myr and n-Myr. The free-radical-scavenging activity was higher for n-Myr at the respective doses compared to that for Myr. The free-radical-scavenging activity was also monitored in zebrafish embryos after treatment with only liposomes, Myr-L, Myr-H, n-Myr-L, and n-Myr-H for 24 h, followed by H₂O₂ treatment (3 mM). The assay was performed immediately and 2 h after H₂O₂ treatment. The results are shown in Figure 3C. Ascorbic acid was taken as a positive control to compare the activity for all these assays.

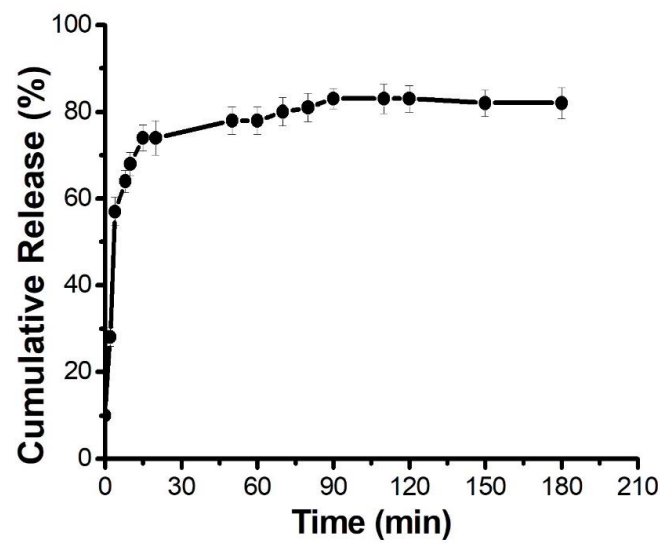


Figure 2. The release of myricetin from the liposomal nanoencapsulation at different time intervals.

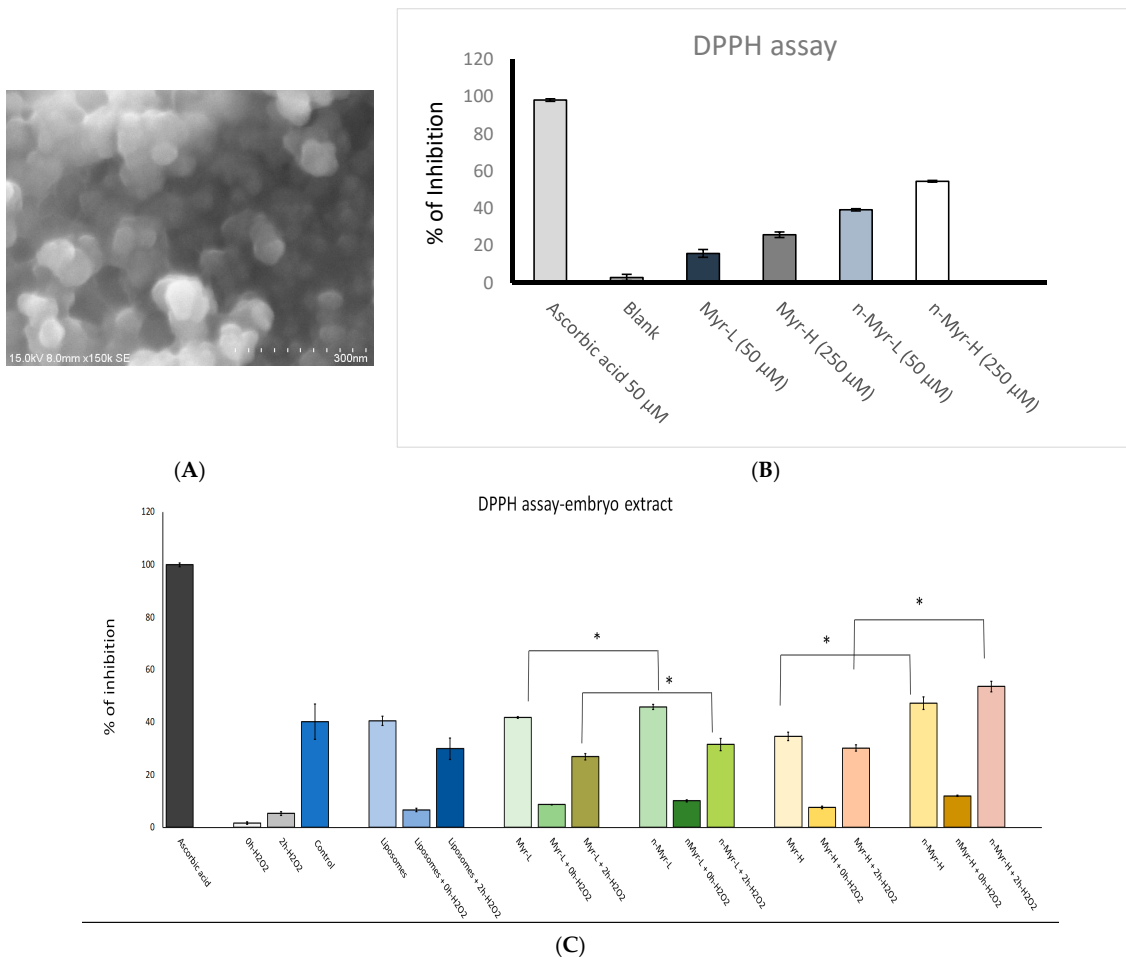


Figure 3. (A) SEM image of liposome-encapsulated myricetin. (B) The percentage inhibition of DPPH by low (50 µM) and high (250 µM) doses of myricetin and liposomal-encapsulated myricetin. Ascorbic acid (50 µM) was taken as a positive control. (C) Zebrafish embryos were treated with only liposomes, Myr-L, Myr-H, n-Myr-L, and n-Myr-H for 24 h. After 24 h, H₂O₂ treatment (3 mM), DPPH radical-scavenging assay was carried out immediately and 2 h after treatment. Untreated embryos were taken as controls for the treated groups, and ascorbic acid was taken as a positive control (* denotes $p < 0.001$).

3.5. Catalase Activity of Zebrafish Embryos

Figure 4A shows the catalase activity of zebrafish embryos without any treatment (control) and after treatment with hydrogen peroxide at 3 mM (oxidative stress). The graph also shows the catalase activity of zebrafish embryos exposed to oxidative stress (hydrogen peroxide, 3 mM) 24 h after treatment with myricetin at low (Myr-L + OS) and high (Myr-H + OS) doses and with liposomal-nanoformulated myricetin at low (n-Myr-L + OS) and high (n-Myr-H + OS) doses. The data showed that after treatment with H_2O_2 , the catalase activity decreased (0.35-fold) in the zebrafish embryos, which reverted to some extent after exposure to low (0.55-fold) and high (0.66-fold) doses of myricetin. However, when exposed to the liposomal-nanoformulated myricetin, the catalase activity reverted to almost normal on low-dose exposure (0.85-fold) and higher than normal in the case of high-dose exposure (1.25-fold).

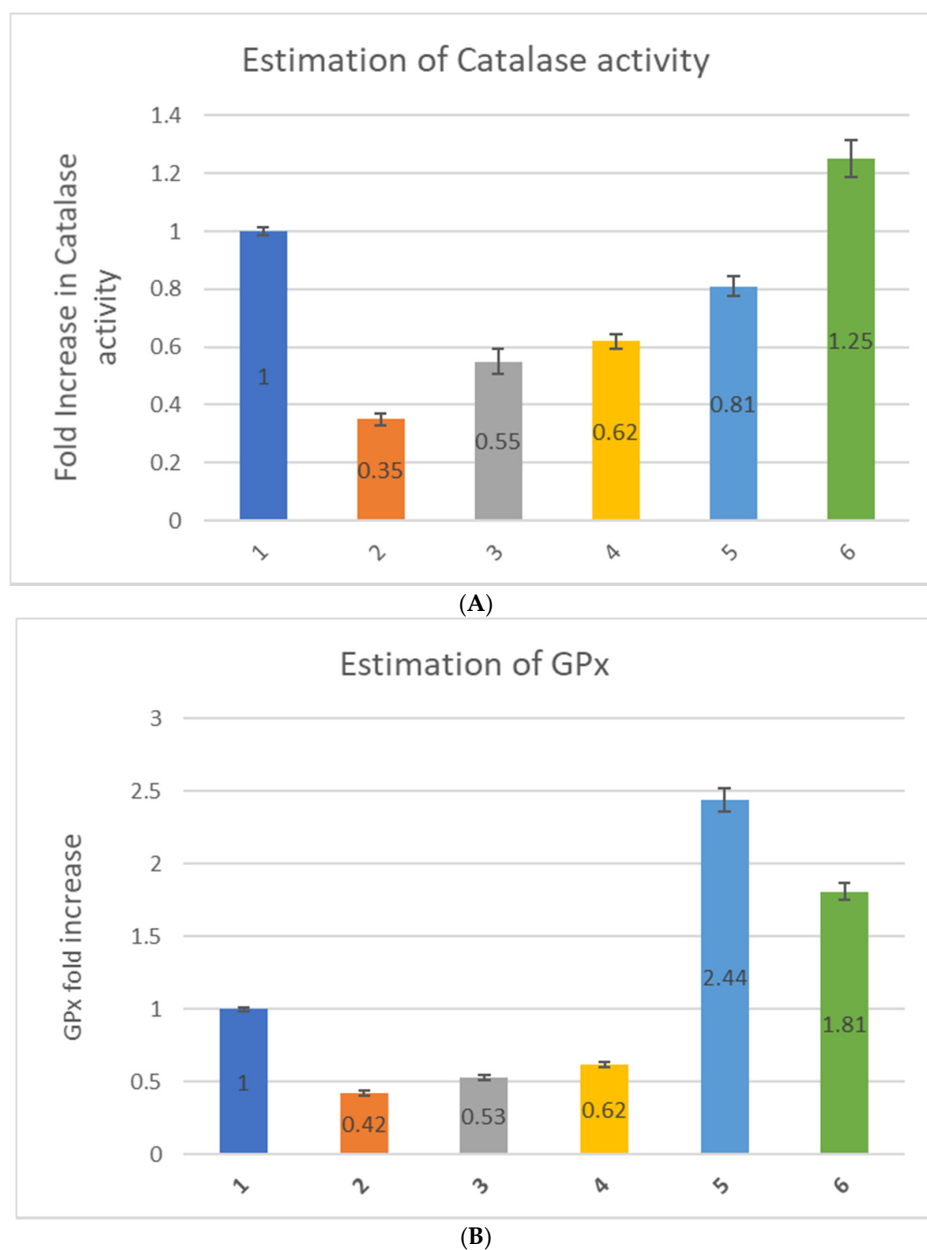


Figure 4. Cont.

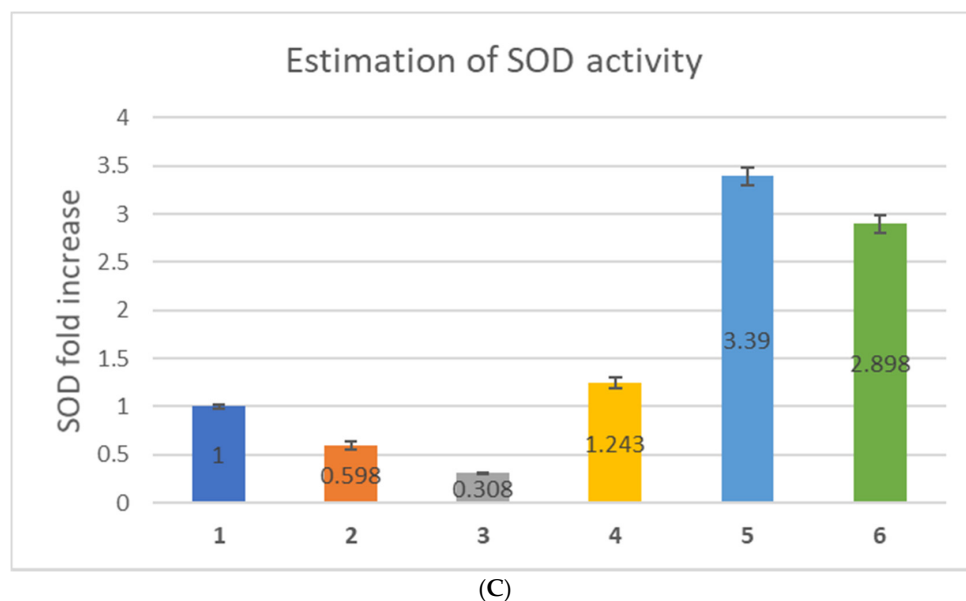


Figure 4. The (A) catalase, (B) glutathione peroxidase, and (C) superoxide dismutase activity of zebrafish embryos without any treatment (control) (1) and after treatment with hydrogen peroxide at 3 mM (oxidative stress) (2). The graph also shows the catalase activity of zebrafish embryos exposed to oxidative stress (hydrogen peroxide, 3 mM) 24 h after treatment with myricetin at low (Myr-L + OS) (3) and high (Myr-H + OS) (4) doses and with liposomal-nanoformulated myricetin at low (n-Myr-L + OS) (5) and high (n-Myr-H + OS) (6) doses.

3.6. Glutathione Peroxidase Activity of Zebrafish Embryos

Figure 4B shows the glutathione peroxidase (GPx) activity of zebrafish embryos without any treatment (control), after treatment with hydrogen peroxide at 3 mM (oxidative stress), and 24 h after treatment with myricetin at low (Myr-L + OS) and high (Myr-H + OS) doses and with liposomal-nanoformulated myricetin at low (n-Myr-L + OS) and high (n-Myr-H + OS) doses and then exposed to oxidative stress (hydrogen peroxide, 3 mM). These results showed that the glutathione peroxidase activity decreased in the zebrafish embryos after exposure to H_2O_2 (0.42-fold), which reverted to some extent after exposure to only myricetin at a low dose (0.53-fold) and a high dose (0.62-fold). However, when exposed to the liposomal-nanoformulated myricetin, the GPx activity was much more enhanced after exposure to a low dose (2.44-fold) and a high dose (1.81-fold).

3.7. Superoxide Dismutase Activity of Zebrafish Embryos

Figure 4C shows the Cu-Zn superoxide dismutase (SOD) activity of zebrafish embryos without any treatment (control), after treatment with hydrogen peroxide at 3 mM (oxidative stress), and 24 h after treatment with myricetin at low (Myr-L + OS) and high (Myr-H + OS) doses and with liposomal nanoformulated myricetin at low (n-Myr-L + OS) and high (n-Myr-H + OS) doses and then exposed to oxidative stress (hydrogen peroxide, 3 mM). These results showed that the SOD activity decreased in the zebrafish embryos after exposure to H_2O_2 (0.598-fold), which further decreased after exposure to a low dose of myricetin (0.308-fold), showing no protection against oxidative stress at this low dose. However, the SOD value reverted after exposure to only myricetin at a high dose (1.243-fold) but when exposed to the liposomal-nanoformulated myricetin, the SOD activity was highly enhanced after exposure to a low dose (3.39-fold) and a high dose (2.89-fold).

3.8. Cumulative Hatchability of Zebrafish Embryos

The effect of myricetin and nanoformulated myricetin without H_2O_2 and after H_2O_2 treatment is shown in Figure 5A,B, respectively. The needle-shaped myricetin particles were visible (deposited) on the embryos at a high-dose treatment at 14 hpf (inset picture

of Figure 5A) with only myricetin. However, there was no such needle-shaped structure observed for nanoformulated-myricetin-treated embryos, both with and without H₂O₂ at both 14 and 36 hpf. After treatment with myricetin and nanoformulated myricetin, the embryos were treated with H₂O₂ and observed under a microscope at 36 hpf. There was the presence of some particles on the embryos for both low and high doses of myricetin, whereas no such particles were visible for the nanoformulated myricetin treatment.

(A) Zebrafish Embryos at 36 and 14 hpf (Inset) after Treatment with Different Doses of Myricetin and Nanoformulated Myricetin 24 h after Treating the Embryos with Different Doses of Myricetin and Nanoformulated Myricetin

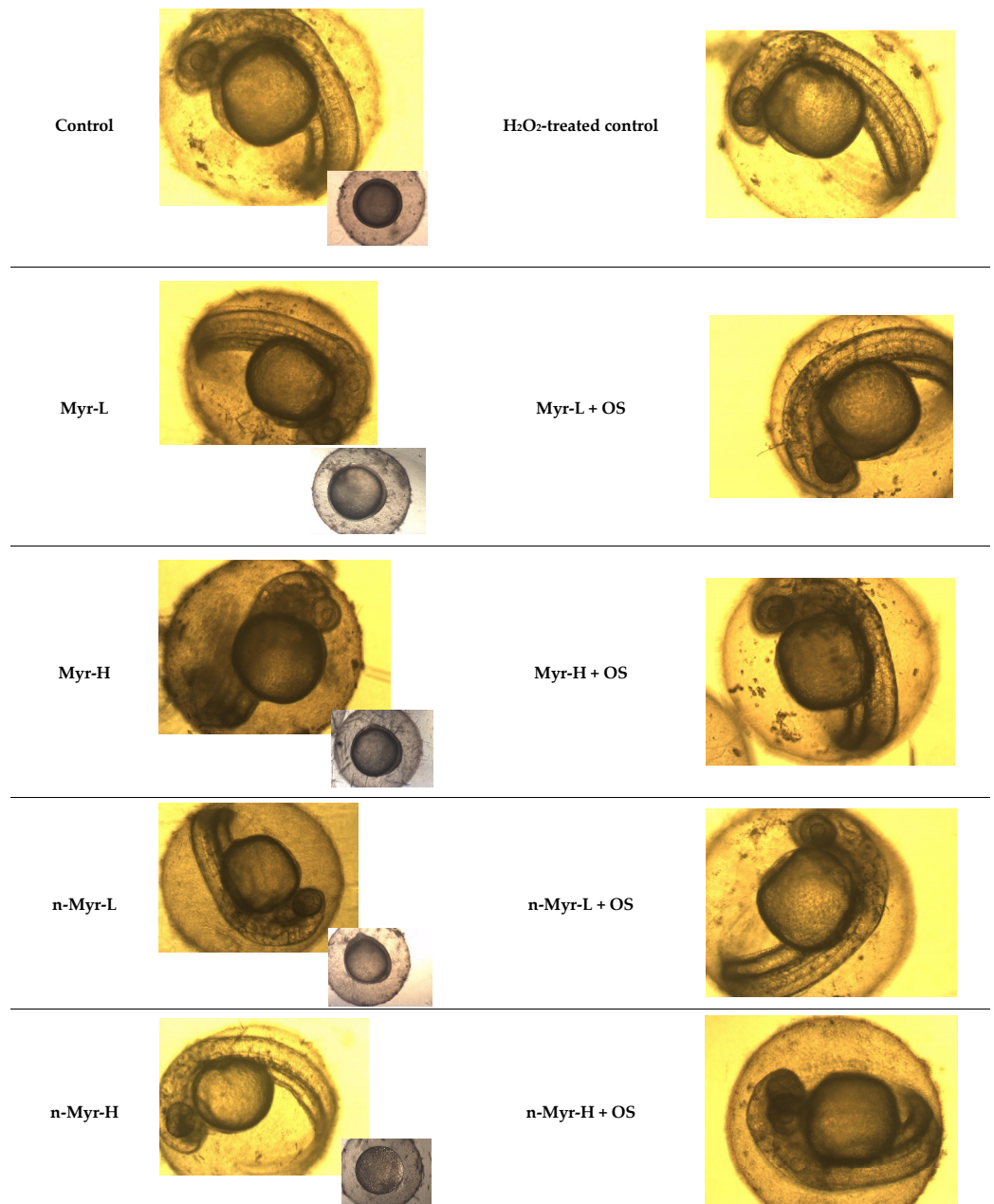


Figure 5. The images of zebrafish embryos after treatment with (A) low and high doses of myricetin (Myr-L and Myr-H) and nanoformulated myricetin (n-Myr-L and n-Myr-H) at 14 hpf (inset) and 36 hpf, respectively. (B) Zebrafish embryos (36 hpf) after treatment with hydrogen peroxide at 3 mM (H₂O₂-treated control) and 24 h after treatment with myricetin at low (Myr-L + OS) and high (Myr-H + OS) doses and with liposomal-nanoformulated myricetin at low (n-Myr-L + OS) and high (n-Myr-H + OS) doses and then exposed to oxidative stress (hydrogen peroxide, 3 mM).

Figure 6 shows the cumulative hatching percentage for hydrogen-peroxide-treated embryos post exposure to myricetin and nano-myricetin treatment at low and high doses. The five groups were H_2O_2 -treated zebrafish embryos as control and H_2O_2 -treated embryos pre-treated with myricetin low dose, myricetin high dose, n-myricetin low dose, and n-myricetin high dose. n-Myricetin-L+ H_2O_2 - and n-myricetin-H+ H_2O_2 -treated zebrafish embryos hatched at the same time. Myricetin-L+ H_2O_2 -treated zebrafish embryos hatched at the same time as myricetin-treated zebrafish embryos at 54 hpf. Myricetin-H+ H_2O_2 -treated zebrafish embryos delayed cumulative hatching, similar to only n-myricetin-H-treated zebrafish embryos.

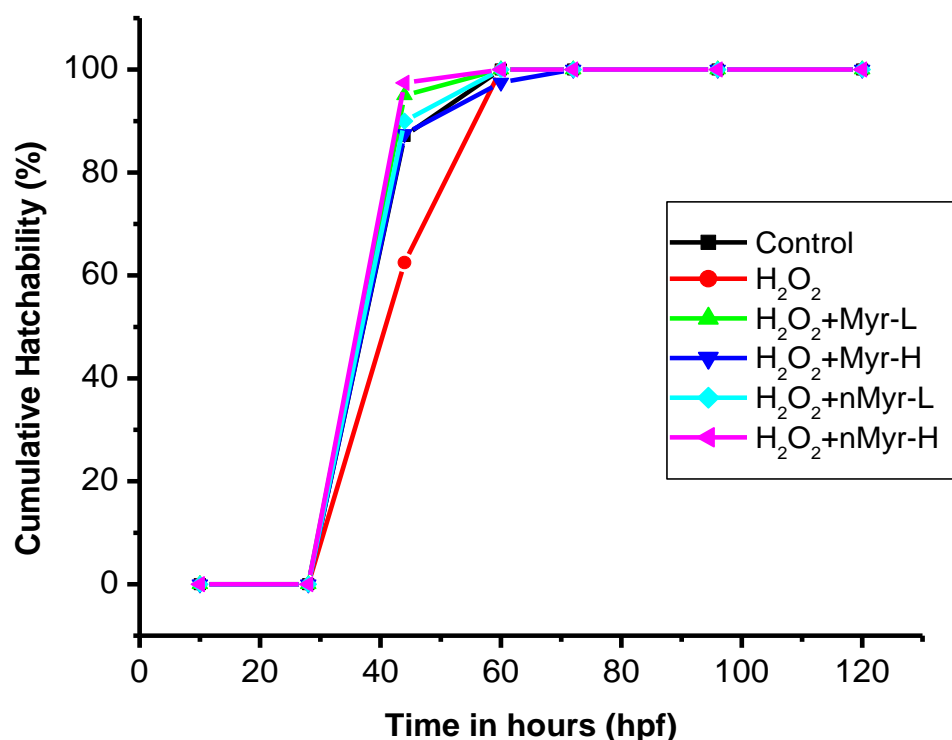


Figure 6. Percentage cumulative hatchability for hydrogen-peroxide-treated embryos after exposure to myricetin and nano-myricetin treatment at low and high doses.

3.9. Developmental Abnormalities in Zebrafish Embryos

Due to the transparency of embryos of zebrafish, we also assessed developmental disabilities in myricetin- and H_2O_2 -treated zebrafish embryos. The images shown in Figure 7 reveal that embryos that were treated with 3 mM H_2O_2 developed pericardial edema, body bend, tail bend, and a higher mortality rate than other group embryos. The embryos treated with nano-myricetin did not show any abnormalities after treatment with hydrogen peroxide at both low as well as high doses of nano-myricetin. A similar finding was also observed for only myricetin.

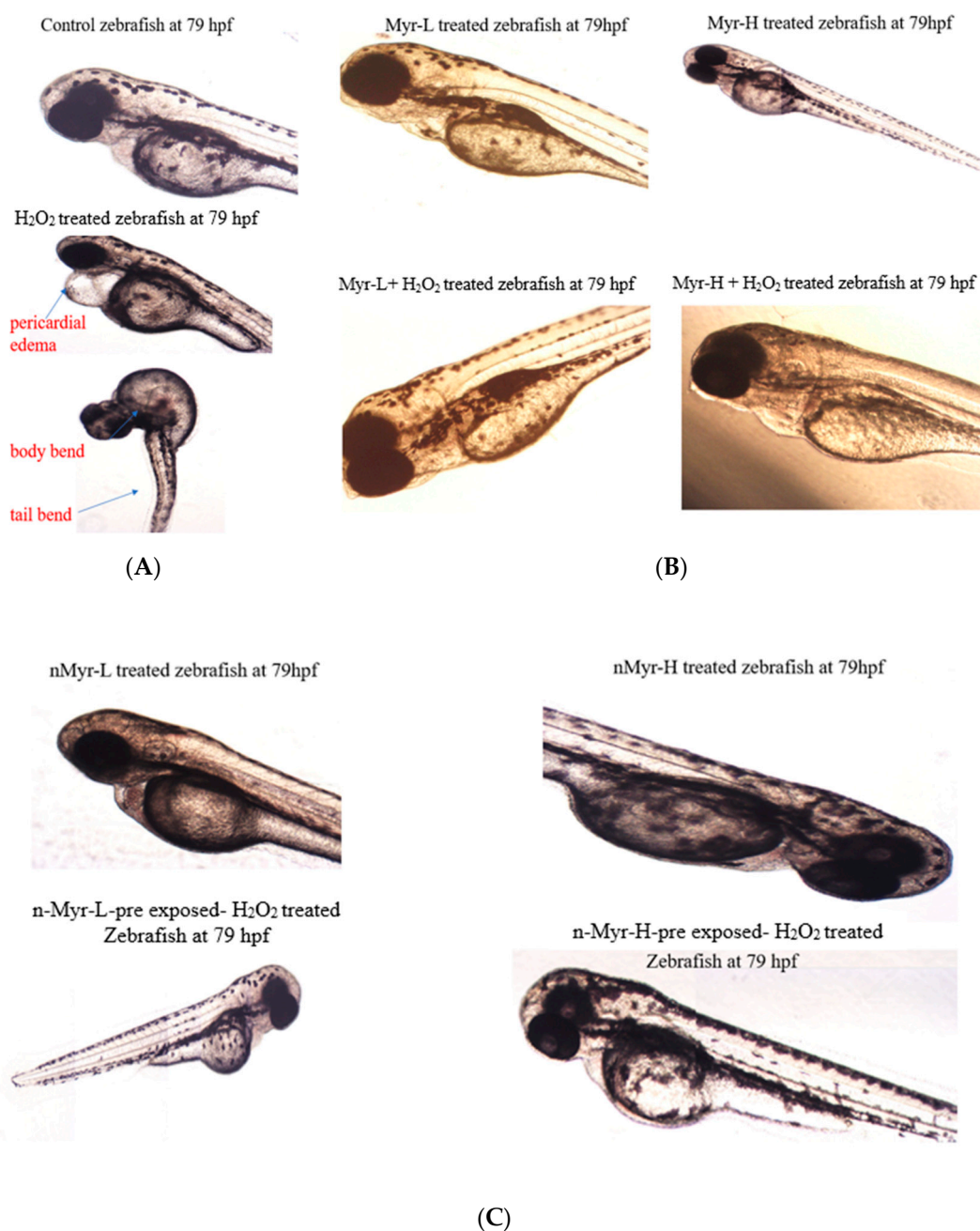


Figure 7. Microscopic images of zebrafish embryos at 79 hpf with developmental disabilities. (A) Control embryos and H₂O₂-treated embryos with abnormalities with pericardial edema, tail bend, and body bend. (B) The zebrafish embryos were treated with low and high doses of myricetin as well as pre-treated with myricetin followed by H₂O₂ treatment. (C) Zebrafish embryos were treated with low and high doses of nano-myricetin followed by hydrogen peroxide treatment. The embryos treated with only hydrogen peroxide without any pre-treatment with myricetin or nano-myricetin were taken as controls.

4. Discussion

Myricetin is abundantly found in fruits and plants and in green tea, black tea, and wine. Myricetin plays a pivotal role in suppressing ROS and anticancer effects *in vitro*, but *in vivo*, due to its low solubility in water, it becomes difficult for it to reach the targeted cells [5]. Nanotechnology has been used for nanoformulations to improve the bioavailability and drug efficacy, as well as being used in the detection of food toxins, biosensors, theranostics, imaging, etc. [22,29–36]. Solid lipid nanoparticles have been used to encapsulate myricetin

to improve its solubility, but they lack biocompatibility to some extent [19]. Myricetin is found to be more potent in inhibiting glutathione reductase (GR) in the presence of O_2^- than in the absence of it. Compared to other flavonols, a minimal concentration (110 μ M) of myricetin inhibited 50% of GR [37]. Myricetin increased GPx activity in Chinese hamster lung fibroblasts (V79-4) cells, as reported in an *in vitro* study [38]. In DSS-induced colitis, murine showed increased GPx and SOD activities [39]. The bioavailability of this polyphenol can be improved with the help of nanotechnology.

A nano-delivery system with a drug or nutraceuticals can better protect the drug from digestive enzymes as well as avoid the loss of the drug before it reaches the target and increase its bioavailability. Different types of nano-delivery systems are available based on the characteristics of a drug, such as liposome encapsulation, solid lipid particles (SLPs), nanostructured lipid carriers, self-dispersing lipid formulations, biopolymer-based delivery systems, and nano-laminated systems. Tang et al. reported myricetin and nano-myricetin encapsulated with Pluronic-based micelles and their effect on glioblastoma cells. It was found that nanoencapsulated myricetin induces higher cytotoxicity in glioblastoma cells than non-encapsulated myricetin [40]. A myricetin nanoformulation with micelles improved ocular anti-inflammatory treatment and improved its stability and solubility [41].

In this work, we used liposomes for the nanoencapsulation of myricetin for improved bioavailability, increased stability, and better solubility. Myricetin possesses needle-like structures when dissolved in PBS (Figure S1), and it may cause damage to the cell wall when interacting with cells. To circumvent this needle-like morphology, it was necessary to encapsulate myricetin inside a nanostructure. The nanoencapsulation was carried out by synthesizing liposomes using the phospholipids isolated from egg yolk and cholesterol. The phospholipid isolation is shown in Figure 1, where we can observe two bands, indicating phosphatidylcholine and phosphatidylethanolamine. Moreover, the absence of any other bands in the chromatogram, which can represent other impurities, such as free fatty acids, free cholesterol, cholesterol esters, or triglycerides, shows that the extraction was of pure phospholipids and there was no other component present in our extract. Previous reports indicate that the two bands in the chromatogram represent phosphatidylcholine and phosphatidylethanolamine and that other impurities (free fatty acids, free cholesterol, cholesterol esters, or triglycerides) are shown in other bands [20]. The drug release kinetics of n-Myr was observed spectrophotometrically (Figure 2). Initially, there was a burst release (up to 30 min), followed by slow release (up to 90 min). After 90 min, myricetin was released in a sustained manner. The encapsulation efficiency of n-Myr was found to be 72%. The synthesized liposomes were observed under a microscope (Figure S2), which showed spherical liposomes. The liposomes were also stable, as visible from the zeta potential value of -30.6 mV (Table 1). The liposome-encapsulated myricetin is shown in Figure S3, where the absence of needle-like structures was observed. The characterization of nano-myricetin was performed using dynamic light scattering, and the results showed that the hydrodynamic diameter of the liposome-encapsulated myricetin was 262 nm, which is in the range defined for nanostructures. The particle was also highly stable, as indicated by the high-magnitude zeta potential of -20.2 mV (Table 1). The surface morphology was visualized by SEM imaging, which showed the spherical nature of the liposomal-encapsulated myricetin, with a diameter of 90 nm to 120 nm (Figure 3A). Thus, the liposomal nanoformulation of myricetin was executed successfully. To establish the free-radical-scavenging activity, a DPPH assay was performed for Myr and for n-Myr. The results showed (Figure 3B) that the free radical scavenging was 39.24% and 54.55% for a low dose and a high dose of n-Myr, respectively. The percentage inhibition was 15.81% and 25.84% for only Myr, respectively. Thus, for each dose, n-Myr exhibited higher free-radical-scavenging activity compared to only Myr. Further, we measured the total antioxidant capability of the embryos pre-treated with low and high doses of Myr and n-Myr (Figure 3C) and further treatment with H_2O_2 . Immediately after H_2O_2 treatment, there was a huge reduction (1.6%) in the radical-scavenging activity in cells that were not treated with Myr or n-Myr. However, 2 h after treatment, there was some improvement

(5.2%) in radical-scavenging activity in cells that were not treated with either Myr or n-Myr. Cells untreated with H₂O₂ or Myr or n-Myr showed similar radical-scavenging activity as that of cells treated with only liposomes, as 40.27% and 40.58%, respectively. The immediate effect of H₂O₂ treatment and the effect 2 h posttreatment was observed for the Myr- and n-Myr-treated embryos, and the results demonstrate that immediate exposure to H₂O₂ caused a reduction in the percentage DPPH inhibition, which resumed after 2 h of treatment. The value returned to nearly that of control cells, but the radical-scavenging activity was significantly higher for all doses of n-Myr compared to Myr.

Further, to explore the effect of only myricetin and nano-myricetin on the antioxidant status of zebrafish embryos, we estimated the antioxidant enzyme activities, such as CAT, GPx, and SOD in zebrafish embryos. CAT activity decreased due to hydrogen peroxide treatment (0.35-fold), which increased to some extent after myricetin treatment. The increase was 0.55-fold after low-dose and 0.62-fold after high-dose treatment with myricetin (Figure 4A). The enhancement was not that pronounced that it could bring back the catalase value similar to that of the control (1-fold). H₂O₂ treatment for n-Myr-L-pre-treated embryos showed improvement in CAT activity nearly similar to control embryos (0.81-fold), and interestingly there was a 25% increase in CAT activity found for n-Myr-H treatment. Thus, nanoencapsulated myricetin can offer protection against oxidative stress by elevating CAT activity. The results of GPx activity were also found to be fascinating. After treatment with hydrogen peroxide, there was a decrease in GPx activity (0.42-fold), which improved after treatment with Myr-L and Myr-H to 0.53- and 0.62-fold, respectively. However, after H₂O₂ exposure to liposome-encapsulated myricetin, there was an increase in GPx activity compared to both Myr-L- and Myr-H-treated zebrafish embryos (Figure 4B). There was a 2.44-fold increase in the GPx level after n-Myr-L treatment and a 1.81-fold increase after treatment with n-Myr-H, showing a huge improvement in GPx activity induced by nanoencapsulated myricetin. The SOD value decreased 0.598-fold after treatment with H₂O₂, which decreased further to 0.308-fold after treatment with Myr-L (Figure 4C). After high-dose treatment with myricetin, the SOD value reverted to that of the control (1.243-fold). In the case of nanoencapsulated myricetin pre-treatment, there was huge protection offered for H₂O₂-exposed zebrafish embryos and the increase in the SOD value was 3.39- and 2.898-fold for n-Myr-L and n-Myr-H, respectively. The results of antioxidant activity showed that the antioxidant enzyme levels decreased after treatment with only myricetin compared to treatment with nanoencapsulated myricetin. Myricetin was found to be 300 times stronger than other flavonoids in inhibiting catalase activity [42]. We have resolved this limitation with liposome-encapsulated myricetin. Low- and high-dose-nano-myricetin-treated embryos expressed more catalase activity after H₂O₂ treatment compared to only low- and high-dose-myricetin-treated zebrafish embryos. From our results, we can speculate that the nanoencapsulation of myricetin could offer better protection against oxidative stress compared to only myricetin.

A step forward, we wanted to monitor the hatching ability of the zebrafish embryos after treatment with H₂O₂ and of myricetin- and nano-myricetin-pre-treated embryos further exposed to H₂O₂. The zebrafish embryos were pre-treated with myricetin as well as nano-myricetin at low and high doses and further exposed to H₂O₂. The images of the zebrafish embryos are shown in Figure 5, and we observed that at 14 hpf, there was an accumulation of needle-shaped myricetin particles on the embryo surface (Figure 5A inset) and also that at 36 hpf, the medium for myricetin-treated samples was more turbid compared to that for samples treated with nanoformulated myricetin. Further, on treatment with H₂O₂, it was revealed that there was a deposition of some particles on the myricetin-treated embryos, which could block the supply of essential nutrients required for the survival of the embryos (Figure 5B). There were no such deposits observed for nano-myricetin-treated embryos. The cumulative hatchability was also calculated for the hydrogen-peroxide-treated embryos (Figure 6). The results showed that after 44 h, hatchability was 87.1% for untreated controls; 62.5% for H₂O₂-treated embryos; and 95% for Myr-L, 87.5% for Myr-H, 90% for n-Myr-L, and 97.4% for n-Myr-H doses. The results of cumulative hatchability

showed that after H₂O₂ treatment, there was delayed hatching, whereas after treatment with myricetin as well as nano-myricetin, the hatching improved and the values were higher than those of the untreated control. When compared at a high dose, n-Myr showed 97.4% hatchability, whereas Myr showed 87.5%, which was significantly lower. After 60 h, there was 100% hatchability observed for all the groups except Myr-H, which showed 97.5% hatchability. Thus, it was observed that at a high dose, the hatchability was delayed for myricetin compared to nano-myricetin and the reason could be the aggregation of myricetin on the eggs, which hinders the exchange of essential nutrients and gases required for the growth and development of the embryos. However, the nanoformulation did not induce any aggregation and the embryos could hatch. A similar finding was observed for ZnO nanoparticles and chitosan-coated ZnO nanoparticles, which showed that ZnO nanoparticle treatment at high doses could induce aggregation on the top layer of the embryos and delay hatching, whereas chitosan coating does not cause any aggregation [24]. Thus, the nanoformulation could protect the embryos from the needle-shaped myricetin particles (Figure S1). Posthatching, we could observe certain developmental abnormalities in the embryos, which are summarized in Figure 7. H₂O₂-treated embryos developed abnormalities in their structures, such as pericardial edema, tail bend, and body bend. In other groups of embryos, such abnormalities were not observed post hatching. The findings from the above study show that liposomal nanoencapsulation of myricetin can improve the antioxidant status and is more biocompatible [43]. Thus, nano-myricetin can impart a superior antioxidant effect as well as enable the healthy development of zebrafish embryos compared to myricetin.

5. Conclusions

In this study, we established that the nanoformulation of myricetin using liposome encapsulation yields improved antioxidant activity. The end point studies were free-radical-scavenging activity of only myricetin and nanoformulated myricetin and antioxidant enzyme activities of zebrafish embryos treated with myricetin and nano-myricetin after H₂O₂ treatment. The free-radical-scavenging activity was higher for nanoencapsulated myricetin compared to that for only myricetin. The nanoformulated liposome-encapsulated myricetin synthesized has a hydrodynamic diameter of about 262 nm and a zeta potential -20 mV, and it ameliorated the activity of the antioxidant enzymes (CAT, GPx, SOD). The formulation was biocompatible, as observed from the cumulative hatchability studies. The drug release kinetics of nano-myricetin showed an initial burst release, followed by slow release, and finally a sustained release pattern. The encapsulation efficiency was 67%, and the surface morphology of nano-myricetin was spherical, having a size of nearly 90 nm. Moreover, liposome-encapsulated myricetin (nano-myricetin) protected zebrafish embryos from developmental disabilities, such as pericardial edema, body bend, and tail bend, that were caused by H₂O₂-induced oxidative stress. Nano-myricetin might be releasing myricetin into the cells in a controlled manner, which can offer protection to the embryos even after 24 h of treatment. Liposomal encapsulation might protect the cells from the pro-oxidant activity of myricetin. However, to demonstrate the exact mechanism of protection of nano-myricetin, future in vivo research is warranted.

Supplementary Materials: The following are available <https://www.mdpi.com/article/10.3390/chemistry4010001/s1>. Figure S1: Microscopic image of myricetin at 400× magnification; Figure S2: Microscopic image of liposomes at 400× magnification; Figure S3: Microscopic image of liposomal encapsulated myricetin at 400× magnification.

Author Contributions: Conceptualization, K.G.; data curation, A.G.; formal analysis, G.A., A.G. and K.G.; funding acquisition, A.G.; methodology, G.A. and K.G.; supervision, K.G.; validation, A.G. and K.G.; writing—original draft, K.G.; writing—review and editing, A.G. All authors have read and agreed to the published version of the manuscript.

Funding: We offer our sincere thanks to the Council of Scientific and Industrial Research (CSIR), INDIA, for the grant (scheme no. 01(2868)/17/EMR-II).

Acknowledgments: The authors are grateful to the Chettinad Academy of Research and Education for supporting the project.

Conflicts of Interest: The authors have no relevant financial or non-financial interests to disclose. The authors have no conflicts of interest to declare that are relevant to the content of this article. All authors certify that they have no affiliations with or involvement in any organization or entity with any financial interest or non-financial interest in the subject matter or materials discussed in this manuscript. The authors have no financial or proprietary interests in any material discussed in this article.

References

1. Ghosh, R.; Girigoswami, K. NADH dehydrogenase subunits are overexpressed in cells exposed repeatedly to H₂O₂. *Mutat. Res.* **2008**, *638*, 210–215. [[CrossRef](#)] [[PubMed](#)]
2. Bose (Girigoswami), K.; Bhaumik, G.; Ghosh, R. Induced resistance in cells exposed to repeated low doses of H₂O₂ involves enhanced activity of antioxidant enzymes. *Cell Biol. Int.* **2005**, *29*, 761–767. [[CrossRef](#)]
3. De, S.; Gopikrishna, A.; Keerthana, V.; Girigoswami, A.; Girigoswami, K. An Overview of Nano formulated Nutraceuticals and its therapeutic approaches. *Curr. Nutr. Food Sci.* **2021**, *17*, 392–407. [[CrossRef](#)]
4. Cory, H.; Passarelli, S.; Szeto, J.; Tamez, M.; Mattei, J. The role of polyphenols in human health and food systems: A mini-review. *Front. Nutr.* **2018**, *5*, 87. [[CrossRef](#)] [[PubMed](#)]
5. Tsao, R. Chemistry and biochemistry of dietary polyphenols. *Nutrients* **2010**, *2*, 1231–1246. [[CrossRef](#)] [[PubMed](#)]
6. Semwal, D.K.; Semwal, R.B.; Combrinck, S.; Viljoen, A. Myricetin: A dietary molecule with diverse biological activities. *Nutrients* **2016**, *8*, 90. [[CrossRef](#)]
7. Devi, K.P.; Rajave, T.; Habtemariam, S.; Nabavi, S.F.; Nabavi, S.M. Molecular mechanisms underlying anticancer effects of myricetin. *Life Sci.* **2015**, *142*, 19–25. [[CrossRef](#)]
8. Ong, K.C.; Khoo, H.E. Biological effects of myricetin. *Gen. Pharmacol.* **1997**, *29*, 121–126. [[CrossRef](#)]
9. Ashrafi, H.; Azadi, A.; Mohammadi-Samani, S.; Hamidi, M. New Candidate Delivery System for Alzheimer’s Disease: Deferoxamine Nanogels. *Biointerface Res. Appl. Chem.* **2020**, *10*, 7106–7119.
10. Rahman, M.M.; Ferdous, K.S.; Ahmed, M. Emerging Promise of Nanoparticle-Based Treatment for Parkinson’s disease. *Biointerface Res. Appl. Chem.* **2020**, *10*, 7135–7151.
11. Bakiro, M.; Hussein Ahmed, S.; Alzamly, A. Effect of pH, Surfactant, and Temperature on Mixed-Phase Structure and Band Gap Properties of BiNbO₄ Nanoparticles Prepared Using Different Routes. *Chemistry* **2019**, *1*, 89–110. [[CrossRef](#)]
12. Zhou, X.; Zhou, M. Polyvinylpyrrolidone-Stabilized Iridium Nanoparticles Catalyzed the Transfer Hydrogenation of Nitrobenzene Using Formic Acid as the Source of Hydrogen. *Chemistry* **2020**, *2*, 960–968. [[CrossRef](#)]
13. Jahanban-Esfahlan, R.; Massoumi, B.; Abbasian, M.; Farnudiyani-Habibi, A.; Samadian, H.; Rezaei, A.; Derakshankhah, H.; Jaymand, M. Dual stimuli-responsive polymeric hollow nanocapsules as “smart” drug delivery system against cancer. *Polym. Plast. Tech. Mat.* **2020**, *59*, 1–13. [[CrossRef](#)]
14. Ahmadi, A.; Hosseini-Nami, S.; Abed, Z.; Beik, J.; Aranda-Lara, L.; Samadian, H.; Morales-Avila, E.; Jaymand, M.; Shakeri-Zadeh, A. Recent advances in ultrasound-triggered drug delivery through lipid-based nanomaterials. *Drug Discov. Today* **2020**, *25*, 2182–2200. [[CrossRef](#)]
15. Azarnezhad, A.; Samadian, H.; Jaymand, M.; Sobhani, M.; Ahmadi, A. Toxicological profile of lipid-based nanostructures: Are they considered as completely safe nanocarriers? *Crit. Rev. Toxicol.* **2020**, *50*, 148–176. [[CrossRef](#)]
16. Gugleva, V.; Ivanova, N.; Sotirova, Y.; Andonova, V. Dermal Drug Delivery of Phytochemicals with Phenolic Structure via Lipid-Based Nanotechnologies. *Pharmaceuticals* **2021**, *14*, 837. [[CrossRef](#)]
17. Alharbi, W.S.; Almughem, F.A.; Almeahady, A.M.; Jarallah, S.J.; Alsharif, W.K.; Alzahrani, N.M.; Alshehri, A.A. Phytosomes as an Emerging Nanotechnology Platform for the Topical Delivery of Bioactive Phytochemicals. *Pharmaceutics* **2021**, *13*, 1475. [[CrossRef](#)]
18. Guo, R.X.; Fu, X.; Chen, J.; Zhou, L.; Chen, G. Preparation and Characterization of Microemulsions of Myricetin for Improving Its Antiproliferative and Antioxidative Activities and Oral Bioavailability. *J. Agric. Food Chem.* **2016**, *64*, 6286–6294. [[CrossRef](#)] [[PubMed](#)]
19. Gaber, D.M.; Nafee, N.; Abdallah, O.Y. Myricetin solid lipid nanoparticles: Stability assurance from system preparation to site of action. *Eur. J. Pharm. Sci.* **2017**, *109*, 569–580. [[CrossRef](#)] [[PubMed](#)]
20. Ramesh, B.; Adkar, S.S.; Prabhudesai, A.V.; Viswanathan, C.V. Selective extraction of phospholipids from egg yolk. *J. Am. Oil Chem. Soc.* **1979**, *56*, 585–587. [[CrossRef](#)] [[PubMed](#)]
21. Vimaladevi, M.; Divya, K.C.; Girigoswami, A. Liposomal nanoformulations of rhodamine for targeted photodynamic inactivation of multidrug resistant gram-negative bacteria in sewage treatment plant. *J. Photochem. Photobiol. B Biol.* **2016**, *162*, 146–152. [[CrossRef](#)] [[PubMed](#)]
22. Deepika, R.; Girigoswami, K.; Murugesan, R.; Girigoswami, A. Influence of Divalent Cation on Morphology and Drug Delivery Efficiency of Mixed Polymer Nanoparticles. *Curr. Drug Deliv.* **2018**, *15*, 652–657. [[CrossRef](#)]
23. Bresciani, E.; Broadbridge, E.; Liu, P.P. An efficient dissociation protocol for generation of single cell suspension from zebrafish embryos and larvae. *MethodsX* **2018**, *5*, 1287–1290. [[CrossRef](#)] [[PubMed](#)]

24. Rajiv, C.; Roy, S.S.; Tamreihao, K.; Kshetri, P.; Singh, T.S.; Sanjita Devi, H.; Sharma, S.K.; Ansari, M.A.; Devi, E.D.; Devi, A.K.; et al. Anticarcinogenic and Antioxidant Action of an Edible Aquatic Flora *Jussiaea repens* L. Using In Vitro Bioassays and In Vivo Zebrafish Model. *Molecules* **2021**, *26*, 2291. [[CrossRef](#)] [[PubMed](#)]
25. Girigoswami, K.; Meenakshi, V.; Murugesan, R.; Girigoswami, A. Studies on Polymer-Coated Zinc Oxide Nanoparticles: UV-blocking Efficacy and in vivo Toxicity. *Mater. Sci. Eng. C* **2015**, *56*, 501–510. [[CrossRef](#)] [[PubMed](#)]
26. Claiborne, A. Catalase activity. In *CRC Handbook of Methods for Oxygen Radical Research*; Greenwald, R.A., Ed.; CRC Press: Boca Raton, FL, USA, 1985; pp. 283–284.
27. Flohé, L.; Günzler, W.A. Assays of glutathione peroxidase. *Methods Enzymol.* **1984**, *105*, 114–121.
28. Paoletti, F.; Mocali, A. Changes in CuZn-superoxide dismutase during induced differentiation of murine erythroleukemia cells. *Cancer Res.* **1988**, *48*, 6674–6677.
29. Sharmiladevi, P.; Breghatha, M.; Dhanavardhini, K.; Priya, R.; Girigoswami, K.; Girigoswami, A. Efficient Wormlike Micelles for the Controlled Delivery of Anticancer Drugs. *Nanosci. Nanotechnol. Asia* **2021**, *11*, 350–356. [[CrossRef](#)]
30. Girigoswami, A.; Mitra Ghosh, M.; Pragma, P.; Seenuvasan, R.; Girigoswami, K. Nanotechnology in Detection of Food Toxin—Focus on the Dairy Products. *Biointerface. Res. Appl. Chem.* **2021**, *11*, 14155–14172.
31. Girigoswami, K.; Girigoswami, A. A Review on Role of Nanosensors in Detecting Cellular miRNA Expression in Colorectal Cancer. *Endocr. Metab. Immune. Disord. Drug Targets* **2021**, *21*, 12–26.
32. Metkar, S.K.; Girigoswami, K. Diagnostic Biosensors in Medicine- a Review. *Biocatal. Agric. Biotech.* **2019**, *17*, 271–283. [[CrossRef](#)]
33. Sharmiladevi, P.; Haribabu, V.; Girigoswami, K.; Abubacker, S.F.; Girigoswami, A. Effect of Mesoporous Nano Water Reservoir on MR Relaxivity. *Sci. Rep.* **2017**, *7*, 11179. [[CrossRef](#)] [[PubMed](#)]
34. Akhtar, N.; Metkar, S.K.; Girigoswami, A.; Girigoswami, K. ZnO nanoflower based sensitive nano-biosensor for amyloid detection. *Mater. Sci. Eng. C* **2017**, *78*, 960–968. [[CrossRef](#)] [[PubMed](#)]
35. Ahmed, B.S.; Mostafa, A.A.; Darwesh, O.M.; Abdel-Rahim, E.A. Development of Specific Nano-Antibody for Application in Selective and Rapid Environmental Diagnoses of *Salmonella arizonae*. *Biointerface Res. Appl. Chem.* **2020**, *10*, 7198–7208.
36. Niri, A.D.; Faridi-Majidi, R.; Saber, R.; Khosravani, M.; Adabi, M. Electrospun carbon nanofiber-based electrochemical biosensor for the detection of hepatitis B virus. *Biointerface Res. Appl. Chem.* **2019**, *9*, 4022–4026.
37. Ellio'it, A.J.; Scheiber, S.A.; Thomas, C.; Pardini, R.S. Inhibition of glutathione reductase by flavonoids- A structure-activity study. *Biochem. Pharmacol.* **1992**, *44*, 1603–1608. [[CrossRef](#)]
38. Wang, Z.H.; Ah Kang, K.; Zhang, R.; Piao, M.J.; Jo, S.H.; Kim, J.S.; Kang, S.S.; Lee, J.S.; Park, D.H.; Hyun, J.W. Myricetin suppresses oxidative stress-induced cell damage via both direct and indirect antioxidant action. *Environ. Toxicol. Pharmacol.* **2010**, *29*, 12–18. [[CrossRef](#)]
39. Zhao, J.; Hong, T.; Dong, M.; Meng, Y.; Mu, J. Protective effect of myricetin, in dextran sulphate sodium-induced murine ulcerative colitis. *Mol. Med. Rep.* **2013**, *7*, 565–570. [[CrossRef](#)]
40. Tang, X.J.; Huang, K.M.; Gui, H.; Wang, J.J.; Lu, J.T.; Dai, L.J.; Zhang, L.; Wang, G. Pluronic-based micelle encapsulation potentiates myricetin-induced cytotoxicity in human glioblastoma cells. *Int. J. Nanomed.* **2016**, *11*, 4991–5002. [[CrossRef](#)]
41. Sun, F.; Zheng, Z.; Lan, J.; Li, X.; Li, M.; Song, K.; Wu, X. New micelle myricetin formulation for ocular delivery: Improved stability, solubility, and ocular anti-inflammatory treatment. *Drug Deliv.* **2019**, *26*, 575–585. [[CrossRef](#)]
42. Krych, J.; Gebicka, L. Catalase is inhibited by flavonoids. *Int. J. Biol. Macromol.* **2013**, *58*, 148–153. [[CrossRef](#)] [[PubMed](#)]
43. Girigoswami, K.; Girigoswami, A.; Murugesan, R.; Agraharam, G. Method and Process of Nanoformulation of Liposomal Myricetin and Uses Thereof. Indian Patent 384885, 22 December 2021.